Nanoscale

COMMUNICATION

View Article Online
View Journal | View Issue

Cite this: *Nanoscale*, 2014, **6**, 11653

Received 29th April 2014
Accepted 4th August 2014

DOI: 10.1039/c4nr02318h

www.rsc.org/nanoscale

A flexible and transparent graphene/ZnO nanorod hybrid structure fabricated by exfoliating a graphite substrate†

Gwang-Hee Nam,‡[a] Seong-Ho Baek,‡[b] Chang-Hee Cho*[c] and Il-Kyu Park*[a]

We demonstrate the fabrication of a graphene/ZnO nanorod (NR) hybrid structure by mechanical exfoliation of ZnO NRs grown on a graphite substrate. We confirmed the existence of graphene sheets on the hybrid structure by analyzing the Raman spectra and current–voltage (*I*–*V*) characteristics. The Raman spectra of the exfoliated graphene/ZnO NR hybrid structure show G and 2D band peaks that are shifted to lower wavenumbers, indicating that the exfoliated graphene layer exists under a significant amount of strain. The *I*–*V* characteristics of the graphene/ZnO NR hybrid structure show current flow through the graphene layer, while no current flow is observed on the ZnO NR/polydimethylsiloxane (PDMS) composite without graphene, thereby indicating that the few-layer graphene was successfully transferred onto the hybrid structure. A piezoelectric nanogenerator is demonstrated by using the fabricated graphene/ZnO NR hybrid structure. The nanogenerator exhibits stable output voltage up to 3.04 V with alternating current output characteristics.

Currently, graphene has attracted much interest for fabricating various functional devices due to its superior properties such as high electron conductivity and mobility, large surface area, high flexibility, and transparency in the visible spectral range.[1–3] Especially, graphene-based semiconductor hybrid nanostructures have received considerable attention for use in optoelectronics,[4–6] photocatalysts,[7–9] photosensors,[10] and water splitting applications.[11] Among the semiconductors, ZnO has been the most widely used because of its large direct bandgap energy of 3.37 eV and high exciton binding energy of 60 meV, giving rise to superior optical properties such as high transparency and efficient ultraviolet (UV) light emission.[12] Furthermore, the easy fabrication of ZnO-based nanostructures with various shapes has made them an attractive basic building block for a wide variety of nano-devices.[12]

Hybridizing these graphene and ZnO nanostructures would be a synergetic way to enhance material properties as well as create a new material system with unique properties. Therefore, many research groups have been investigating the fabrication of graphene/ZnO nanorod (NR) hybrid structures *via* seeded solution growth methods, chemical vapor deposition (CVD), the chemical conversion method, and the preparation of carbon layers.[4–10] For example, the hybrid graphene/ZnO NR structure has been achieved with a CVD-grown graphene which was transferred from a foreign substrate to form the hybrid structure.[13] In the case of graphene oxide (GO)/ZnO NR, it suffers from poor electrical conductivity by defects in GO, and therefore reduction processes are required in the experimental procedure.[14,15] In this work, we investigate a novel approach to form a graphene/ZnO NR hybrid structure. ZnO NRs are grown on a highly oriented pyrolytic graphite (HOPG) substrate directly and a polymer-assisted mechanical exfoliation produces the graphene/ZnO NR hybrid structure. Taking advantage of this approach, the HOPG substrate can be recycled after the exfoliation of the graphene/ZnO NR composite. In order to demonstrate the usefulness of the graphene/ZnO NR hybrid structure in device applications, we fabricated a fully flexible piezoelectric nanogenerator in which the exfoliated graphene layers work as an electrode material.

Graphene/ZnO NR composites were obtained by mechanical exfoliation of hydrothermally grown ZnO NRs on a graphite substrate, as shown schematically in Fig. 1. ZnO NRs were grown on HOPG substrates by a two-step hydrothermal method involving the formation of a ZnO seed layer. This was followed by the growth of the main ZnO NR layer. The ZnO seed layer was formed by dipping the graphite substrate into 40 mM zinc acetate dihydrate ($Zn(CH_3COO)_2 \cdot 2H_2O$) dissolved in ethanol solution, followed by drying at 100 °C for 5 min. The main ZnO NR layer was grown on the seed layer coated on the graphite

[a]*Department of Electronic Engineering, Yeungnam University, Gyeongbuk 712-749, South Korea. E-mail: ikpark@ynu.ac.kr*

[b]*Energy Research Division, Daegu Gyeongbuk Institute of Science & Technology (DGIST), Daegu 711-873, South Korea*

[c]*Department of Emerging Materials Science, Daegu Gyeongbuk Institute of Science & Technology (DGIST), Daegu 711-873, South Korea. E-mail: chcho@dgist.ac.kr*

† Electronic supplementary information (ESI) available. See DOI: 10.1039/c4nr02318h

‡ These authors contributed equally to this work.

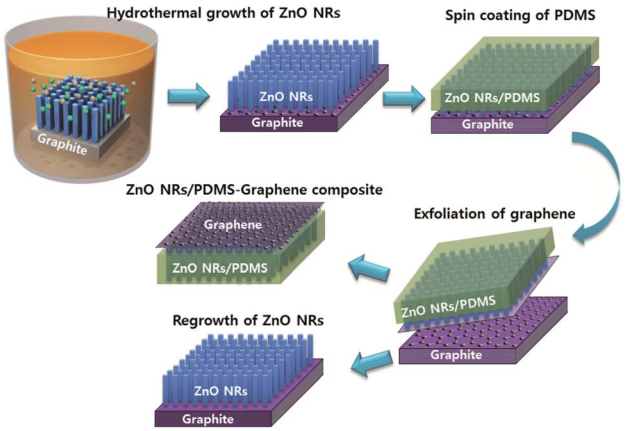

Fig. 1 Schematic of processing steps for the fabrication of the graphene/ZnO NR hybrid structure using mechanical exfoliation of PDMS-coated ZnO NRs grown on a graphite substrate.

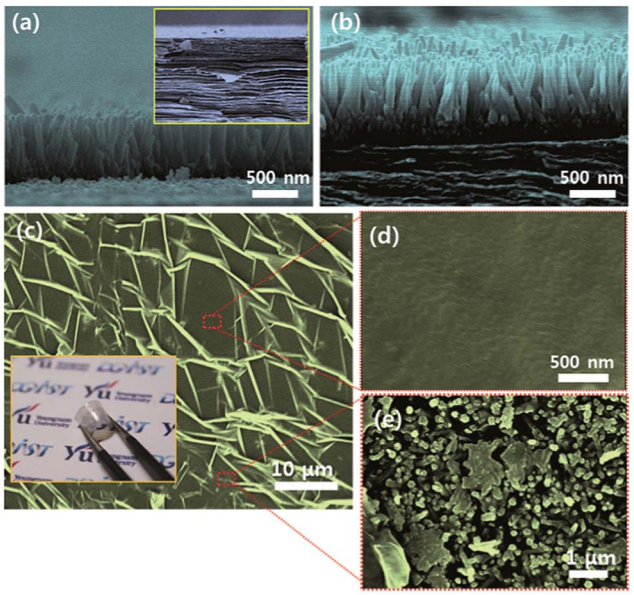

Fig. 2 FE-SEM images of (a) the as-grown ZnO NRs on a graphite substrate. The inset shows a cross-sectional image of the graphite substrate composed of multiple graphene sheets. (b) Re-grown ZnO NRs on a previously exfoliated graphite substrate. (c) The surface of the graphene/ZnO NRs after exfoliation. The inset shows the exfoliated free-standing graphene/ZnO NR composite. (d) Enlarged image of the top surface of the graphene/ZnO NRs showing a wrinkle pattern on the exfoliated graphene layer and (e) showing a local open area in the absence of the graphene layer.

substrate in an aqueous solution of 40 mM zinc nitrate hexahydrate ($Zn(NO_3)_2 \cdot 6H_2O$) and 40 mM hexamine ($(CH_2)_6N_4$; HMT) at 90 °C for 3 h, followed by cleaning in running deionized (DI) water for 5 min. Then, polydimethylsiloxane (PDMS) was spin-coated onto the ZnO NRs on the graphite substrate. Here, PDMS acts as a flexible support for the exfoliated composite during or after the exfoliation process. The PDMS (Sylgard 184) pre-polymer to cross-linker (curing agent) ratio was 10 : 1 without dilution. The spin rate was kept constant at 4000 rpm for 150 s, which resulted in an ~4 μm thick PDMS film on a flat substrate using the same conditions. Subsequently, the sample was placed in a vacuum chamber with a pressure of 0.2 Torr for 10 min to remove the trapped air bubbles between the ZnO NRs and PDMS. This procedure improves the penetration of PDMS into the ZnO NRs and thereby enhancing the adhesion between the ZnO NRs and PDMS. Finally, curing of the sample was performed at 70 °C for 2 h in an oven. The ZnO NR/PDMS coating layer was mechanically exfoliated from the graphite substrate by carefully peeling it off with a set of tweezers under a microscope. After the exfoliation, the surface of the graphite substrate was clear, thereby indicating that the ZnO NRs transferred from the substrate into the exfoliated PDMS. To confirm the recycling of the graphite substrate, the growth procedure of the ZnO NRs was repeated on the exfoliated graphite substrate.

The structural properties were examined using field emission-scanning electron microscopy (FE-SEM). In order to confirm the successful exfoliation of graphene with ZnO NRs, Raman spectroscopy was carried out with 532 nm laser excitation. The optical properties of the ZnO NRs were investigated by photoluminescence (PL) spectroscopy, in which a 325 nm continuous He–Cd laser was used as an excitation source at room temperature. The electrical properties of the graphene/ZnO NR hybrid structures were measured using a source meter (Keithley 2612).

Fig. 2 shows FE-SEM images of the ZnO NRs grown on the graphite substrate and the graphene/ZnO NR hybrid structure. As shown in Fig. 2(a), the diameter of the ZnO NRs is estimated to be about 50 nm. The inset of Fig. 2(a) shows a cross-sectional image of the broken graphite substrate, which is composed of multilayer graphene sheets. Since the graphitic surface has no reactive dangling bonds, the binding mechanism between the ZnO and graphene has been known to be a quasi-van der Waals binding.[16] By taking the semiconductor atoms on favorable sites of the graphitic surface such as the center of the hexagonal carbon rings or the bridge between two carbon atoms, the lattice-matched arrangement of semiconductor atoms on the graphitic surface becomes possible. In particular, ZnO has a very small lattice mismatch with the graphitic surface for such an atomic configuration, resulting in the epitaxial growth of ZnO NRs on the graphite substrate.[16] Fig. 2(b) shows the ZnO NRs grown again on the graphite substrate after exfoliating the ZnO NR/PDMS layer to confirm the feasibility of recycling the graphite substrate. The surface morphologies of the ZnO NRs on both substrates before and after the exfoliation are similar. This indicates that the graphite substrate can be reused repeatedly to fabricate the nanostructure/graphene composite. Fig. 2(c) shows the surface of the graphene/ZnO NRs embedded in PDMS after exfoliation. The surface of the graphene side shows many wrinkles that were generated during the mechanical exfoliation process due to biaxial strain on a PDMS polymer support.[17] The enlarged image of the top surface shows a water wave pattern on the exfoliated graphene layer (Fig. 2(d)), whereas local open areas also exist in which the graphene layer is absent because of the poor adhesion problem of ZnO NRs to the graphite substrate where the ZnO seed layer was not formed

well (Fig. 2(e)). The inset of Fig. 2(c) shows an image of a detached free-standing graphene/ZnO NR composite that is flexible and transparent. The shear stress required to exfoliate the graphene from the graphite is sufficient to overcome the weak van der Waals interactions between the graphene layers of the graphite substrate. The ZnO NRs on graphene have been known to be mechanically stable at an atomic level which has been verified through the first principles calculations.[18]

In order to investigate the optical and strain properties of transferred ZnO NRs, PL spectra were measured for as-grown and PDMS-coated ZnO NRs as well as the ZnO NR/graphene composite after the exfoliation, as shown in Fig. 3. The PL spectra of all samples exhibit two main emission bands: a sharp peak in the ultraviolet range (379 nm) and a broad peak (620 nm) in the visible range. These peaks correspond to the band edge emission of a ZnO semiconductor and deep level-related emissions, respectively, as shown in the inset of Fig. 3. The ZnO NRs after PDMS coating show a spectrum similar to that of the as-grown ZnO NRs on the graphite substrate, whereas the deep level emission is suppressed after embedding the PDMS. This would be due to the suppression of surface-related defects by passivating the ZnO NRs. After exfoliating the ZnO NR/PDMS from the graphite, no emission was observed on the remaining graphite substrate due to the complete removal of the ZnO NRs. This indicates the successful transfer of the ZnO NRs into the PDMS matrix. The transferred ZnO NR/PDMS composite shows a similar feature to that of the as-grown ZnO NRs and PDMS-coated ZnO NRs on the graphite substrate, except that the band edge emission peak was red-shifted by 7 nm. This can be explained by a decrease in the bandgap energy of ZnO (see Fig. S1 in the ESI†), resulting from biaxial compressive strain (and thus uniaxial tensile strain along the *c*-axis), which would be induced by an elastomeric property of the PDMS embedding the ZnO NRs.[19] Note that the highest PL intensity in the exfoliated ZnO NR/PDMS composite can be due to the absence of the graphite substrate, which absorbs a significant amount of emitted light.[20] The PL results show that the ZnO NR/PDMS layer was successfully transferred from the graphite substrate, with the biaxial compressive strain induced into the ZnO NRs as a result of being embedded in the PDMS.

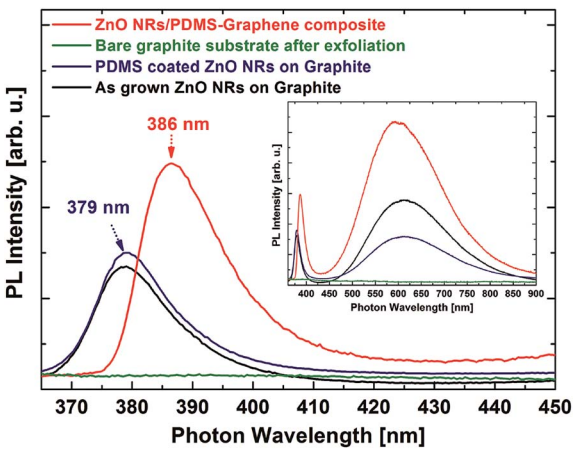

Fig. 3 PL spectra measured at room temperature for as-grown ZnO NRs, PDMS-coated ZnO NRs on the graphite substrate, and the graphene/ZnO NR composite after exfoliation. The PL for the bare graphite substrate after exfoliation was measured to confirm the complete removal of the ZnO NRs.

Fig. 4(a) shows the Raman spectra of the as-grown ZnO NRs on the graphite substrate, and the transferred ZnO NR/PDMS composite. The Raman spectra of all samples show similar spectral shapes with two main Raman-active regions: one for ZnO NRs and the other for carbon-related components. Fig. 4(b) shows the detailed Raman spectra around ZnO peaks for the as-grown ZnO NRs on the graphite substrate, and the transferred ZnO NR/PDMS composite. ZnO has a wurtzite crystal structure belonging to the C_{6v}^4 space group. As-grown ZnO NRs on graphite mainly show two peaks at 334 and 435 cm^{-1} which are assigned as $E_2^{high} - E_2^{low}$ and E_2^{high}, respectively.[21] Two shoulder peaks near E_2^{high} correspond to the transverse optic (TO) component, which indicates that the ZnO NRs are highly crystalline. The transferred ZnO NRs embedded in the PDMS layer show one peak at 493 cm^{-1}, corresponding to the E_2^{high} mode, which is attributed to atomic displacements perpendicular to the *c*-axis. The vibrational energy is strongly affected by the biaxial strain, which also gives rise to a change in the exciton energy of ZnO. In a hexagonal system, the amount of strain (ε_{cc}) along the *c*-direction can be estimated from the shift in the E_2^{high} peak position ($\Delta\omega$),[22] which is given by

$$\Delta\omega = \left[b - a\left(\frac{C_{33}}{C_{13}}\right)\right]\varepsilon_{cc}$$

where b and a are phonon deformation potential parameters, and C_{33} and C_{13} are the elastic constants. The shift of the E_2^{high} peak after being transferred from the graphite is 58 cm^{-1}. This indicates that the strain state was changed significantly by the biaxial compressive stress. We believe that the biaxial strain can be introduced due to the elastomeric characteristics of the embedding PDMS polymer. We note that this change in the strain state in ZnO NRs by embedding in PDMS is consistent with the PL results.

To determine the existence of the graphene layer at the bottom surface of the ZnO NR/PDMS composite exfoliated from the graphite substrate, Raman spectroscopy was also carried out for the spectral region of the G and 2D bands, as shown in Fig. 4(c) and (d), respectively. Two intense peaks at ~1583 cm^{-1} (G) and ~2700 cm^{-1} (2D) are the typical features of graphite and multilayer graphene. The representative G and 2D peaks are observed in the exfoliated ZnO NRs/PDMS composite, which clearly indicates that the graphene layers exist and is composed of few-layer graphene.[23] However, both the G and 2D peaks shifted to lower wavenumbers for the exfoliated ZnO NR/PDMS composite, showing the G band down-shifted by 14 cm^{-1} and the 2D band down-shifted by 23 cm^{-1} compared to those of the graphite with as-grown ZnO NRs. This strongly suggests that the graphene layers experienced a significant amount of strain since they were formed through a heterostructure with the ZnO NR/PDMS composite, which includes thermal heating and cooling processes in the fabrication procedure. It has been reported that graphene-based heterostructures give rise to an

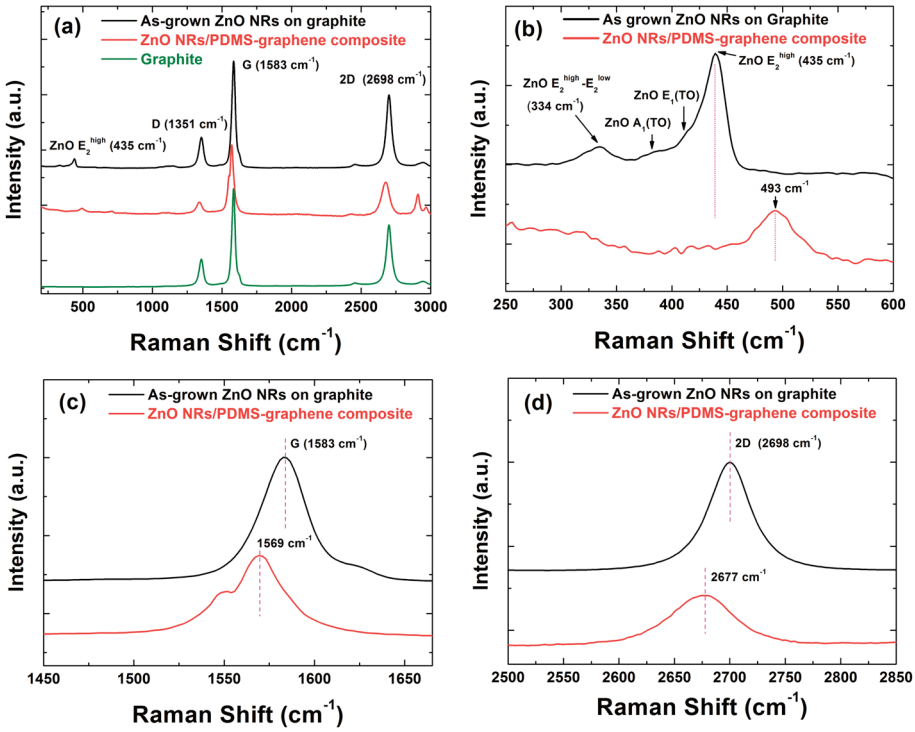

Fig. 4 (a) Raman spectra measured at room temperature for as-grown ZnO NRs on the graphite substrate, and the graphene/ZnO NR composite after exfoliation. Raman spectrum of graphite is also shown for a comparison. Detailed Raman spectra of (b) the ZnO NRs, (c) the G band of graphite/graphene, and (d) the 2D band of graphite/graphene.

inhomogeneous strain distribution that is likely due to the mismatch of their thermal expansion coefficients.[24] From the Raman spectra, even though it was difficult to identify the number of graphene layers on the exfoliated sample due to the complex effect of the strain and the layer number, we confirmed that the graphene on the ZnO NR/PDMS was successfully transferred from the graphite substrate as seen in X-ray diffraction and transmission electron microscopy results (see Fig. S2 in the ESI†). Furthermore, the exfoliated graphene has a good crystal quality which is comparable with the bulk graphite substrate. The defect density of graphene can be evaluated from the D to G peak intensity ratio of Raman spectrum since the ratio is inversely proportional to the crystallite size.[25] When compared to reduced graphene oxide/ZnO NR composites,[14,15] the exfoliated graphene would have better crystallinity, as confirmed by the D to G peak intensity ratio. In comparison between the Raman spectra of the as-grown ZnO NRs on graphite and the bulk graphite (Fig. 4(a)), the D to G peak intensity ratios are estimated to be almost the same (~0.27), showing that the crystal quality of graphite does not change due to the growth of ZnO NRs. More importantly, the exfoliated graphene/ZnO NR composite also shows such a low level of D to G peak ratio (~0.18), indicating that the exfoliated graphene layer still maintains the crystal quality.

To confirm the electrical properties and the validity for device applications of the proposed ZnO NR/PDMS with graphene, current–voltage (I–V) characteristics were measured for the exfoliated graphene/ZnO NR hybrid structures. The contact electrodes were fabricated by using indium metal balls with a spherical shape, and without any patterning and thermal annealing processes to avoid surface modification during the formation of the metal electrodes, which can occur during the photolithography and thin film processes. To compare the electrical properties of the ZnO NR/PDMS layer with and without the graphene layer on the surface, a ZnO NR/PDMS composite without the graphene layer was fabricated by exfoliating the PDMS-coated ZnO NRs grown on a Si (100) substrate. As shown in Fig. 5, no current flowed on the ZnO

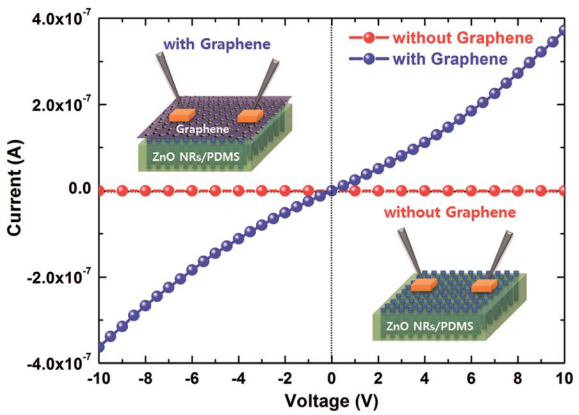

Fig. 5 The I–V characteristics of the ZnO NR/PDMS layer with and without the graphene layer on the surface. The insets show a schematic of the device structure for I–V measurement.

NRs/PDMS composite without the graphene, whereas a significant amount of current flowed on the sample with the graphene layer. The series resistance of the heterostructures was estimated by using $I\mathrm{d}V/\mathrm{d}I = R_S I + k_B T/e$, where R_s and e are the series resistance of the devices and the electron unit charge, respectively. The ZnO NR/PDMS with the graphene layer showed a high series resistance of 22.9 MΩ, which was probably due to the non-optimal metal contacts, wrinkles on the graphene surface, and the imperfect graphene coverage, as shown in the FE-SEM images. However, this result clearly indicates that the graphene layer exists at the bottom of the ZnO NRs which were exfoliated from the graphite substrate. The graphene layer can also be utilized for a transparent metallic electrode.

As shown in the inset of Fig. 2(c), the exfoliated ZnO NR/PDMS with graphene is transparent and highly flexible, which enables us to extend the benefits by using a ZnO NR/graphene composite in many applications such as optoelectronic and energy conversion devices. Especially, this approach is suitable for a transparent and flexible piezoelectric energy generator with high efficiency. To this end, we demonstrated a piezoelectric nanogenerator based on a ZnO NR/PDMS composite with a graphene electrode. Fig. 6 shows the piezoelectric output potential results of the ZnO NR/PDMS-based piezoelectric nanogenerator with a graphene electrode. The input mechanical force was driven by a cylindrical rod with a diameter of 5 mm, connected to a motorized cam. By adjusting the voltage of the motor rotating the cam, the frequency of the input mechanical force was controlled from 1.6 to 3.4 Hz. The time-dependent output voltage was recorded using an oscilloscope. As shown in Fig. 6(a), the piezoelectric nanogenerator showed a stable output voltage above 3 V with an alternating current output signal. Fig. 6(c) shows that the output voltage increased from 1.6 to 3.04 V as the frequency of the input mechanical force increased from 1.6 to 3.4 Hz. The output voltage generated from the piezoelectric nanogenerator increases linearly as the force (F) increases, and the output voltage is given by[26]

$$V = \frac{\mathrm{d}L}{\varepsilon_r \varepsilon_0 A} F$$

where d, ε_r, ε_0, L, and A are the piezoelectric constant and the relative dielectric constant of the piezoelectric material, the dielectric constant of the vacuum, the length, and the cross-sectional area of the device, respectively. These are the typical characteristics of the piezoelectric nanogenerator.[27] Our results for the piezoelectric energy generator demonstrate the validity of potential device applications using the proposed flexible and transparent graphene/ZnO NR hybrid structures.

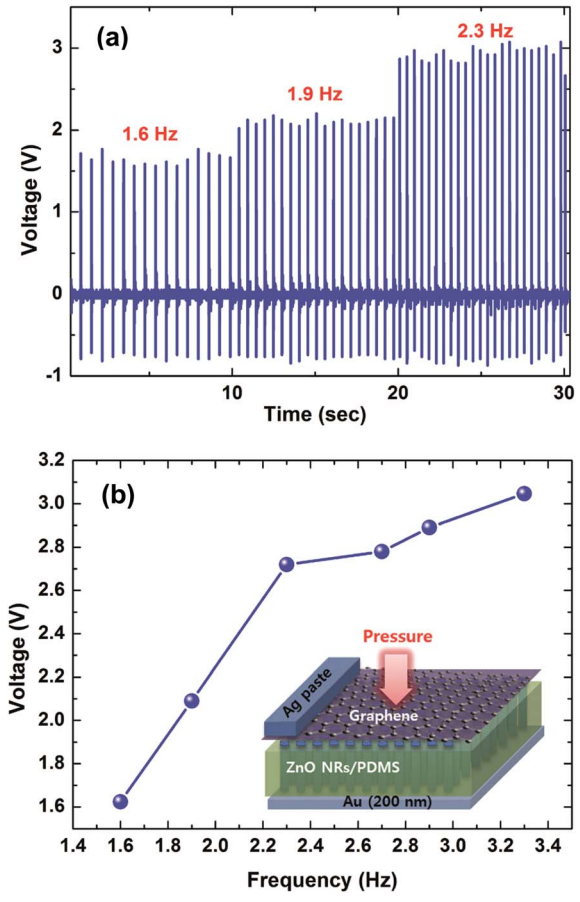

Fig. 6 (a) Piezoelectric output potential measured from the ZnO NR/PDMS-based piezoelectric nanogenerator with an exfoliated graphene electrode. (b) Output voltage with variation of the frequency of the input mechanical force. The inset shows a schematic of the device structure.

In summary, we demonstrated an innovative approach for fabricating a graphene/ZnO NR hybrid structure by means of mechanical exfoliation of ZnO NRs grown on a graphite substrate. A structural investigation using FE-SEM showed that the ZnO NRs embedded in PDMS were successfully transferred by the mechanical exfoliation process due to weak van der Waals interactions between the graphene sheets in the graphite. The PL spectra showed that the ZnO NRs were completely removed from the graphite substrate after the exfoliation process and were under uniaxial tensile strain along the c-axis, which was induced by the elastomeric property of the PDMS embedding the ZnO NRs. The Raman spectra of the exfoliated ZnO NR/graphene hybrid structure show G and 2D band peaks that shifted to a lower wavenumber. This indicates that the few-layer graphene exists at the surface of the ZnO NRs embedded in the PDMS. The I–V characteristics of the graphene/ZnO NR hybrid structure showed current flow through the graphene layer, whereas no current flowed on the ZnO NR/PDMS composite without the graphene layer. This indicates that the graphene layer was successfully transferred onto the hybrid structure. A transparent and flexible piezoelectric nanogenerator was demonstrated by using a graphene/ZnO NR hybrid structure. The piezoelectric nanogenerator showed a stable output voltage of up to 3 V with alternating current output characteristics. The proposed approach is expected to provide a viable way of recycling expensive graphite substrates, and of fabricating a semiconductor nanostructure/graphene hybrid structure. These advantages have considerable potential for applications in a wide range of flexible devices.

Acknowledgements

This research was supported by the Basic Science Research Program (2012R1A1A1001711 and 2013R1A1A1009552) and the Leading Foreign Research Institute Recruitment Program (2012K1A4A3053565) through the National Research Foundation of Korea, and by DGIST R&D Program (14-BD-0401, 14-EN-01) funded by the Ministry of Science, ICT and Future Planning of the Korean government.

References

1 A. K. Geim and K. S. Novoselov, *Nat. Mater.*, 2007, **6**, 183–191.
2 S. Garaj, W. Hubbard, A. Reina, J. Kong, D. Branton and J. A. Golovchenko, *Nature*, 2010, **467**, 190–193.
3 Y. Zhang, Y. W. Tan, H. L. Stormer and P. Kim, *Nature*, 2005, **438**, 201–204.
4 J. Chen, C. Li, G. Eda, Y. Zhang, W. Lei, M. Chhowalla, W. I. Milne and W.-Q. Deng, *Chem. Commun.*, 2011, **47**, 6084–6086.
5 M. K. Kim, D. K. Yi and U. Paik, *Langmuir*, 2010, **26**, 7552–7554.
6 J. M. Lee, Y. B. Pyun, J. Yi, J. W. Choung and W. I. Park, *J. Phys. Chem. C*, 2009, **113**, 19134–19138.
7 Z. Chen, N. Zhang and Y.-J. Xu, *CrystEngComm*, 2013, **15**, 3022–3030.
8 N. Zhang, Y. Zhang and Y.-J. Xu, *Nanoscale*, 2012, **4**, 5792–5813.
9 N. Zhang, M.-Q. Yang, Z.-R. Tang and Y.-J. Xu, *ACS Nano*, 2014, **8**, 623–633.
10 H. Chang, Z. Sun, K. Y.-F. Ho, X. Tao, F. Yan, W.-M. Kwok and Z. Zheng, *Nanoscale*, 2011, **3**, 258–264.
11 Q. Xiang, J. Yu and M. Jaroniec, *Chem. Soc. Rev.*, 2012, **41**, 782–796.
12 Z. L. Wang, *J. Phys.: Condens. Matter*, 2004, **16**, R829–R858.
13 D. Choi, M. Y. Choi, W. M. Choi, H. J. Shin, H. K. Park, J. S. Seo, J. Park, S.-M. Yoon, S. J. Chae, Y. H. Lee, S. W. Kim, J. Y. Choi, S. Y. Lee and J. M. Kim, *Adv. Mater.*, 2010, **22**, 2187–2192.
14 Z. Yin, S. Wu, X. Zhou, X. Huang, Q. Zhang, F. Boey and H. Zhang, *Small*, 2010, **6**, 307–312.
15 U. Alver, W. Zhou, A. B. Belay, R. Krueger, K. O. Davis and N. S. Hickman, *Appl. Surf. Sci.*, 2012, **258**, 3109–3114.
16 A. M. Munshi, D. L. Dheeraj, V. T. Fauske, D. C. Kim, A. T. J. van Helvoort, B. O. Fimland and H. Weman, *Nano Lett.*, 2012, **12**, 4570–4576.
17 J. Zang, S. Ryu, N. Pugno, Q. Wang, Q. Tu, M. J. Buehler and X. Zhao, *Nat. Mater.*, 2013, **12**, 321–325.
18 W. M. Choi, K. S. Shin, H. S. Lee, D. Choi, K. Kim, H. J. Shin, S. M. Yoon, J. Y. Choi and S. W. Kim, *Nano Res.*, 2011, **4**, 440–447.
19 C. P. Dietrich, M. Lange, F. J. Klüpfel, H. von Wenckstern, R. Schmidt-Grund and M. Grundmann, *Appl. Phys. Lett.*, 2011, **98**, 031105.
20 J. M. Zhang and P. C. Eklund, *J. Mater. Res.*, 1987, **2**, 858–863.
21 S. Sahoo, G. L. Sharma and R. S. Katiyar, *J. Raman Spectrosc.*, 2012, **43**, 72–75.
22 R. J. Briggs and A. K. Ramdas, *Phys. Rev. B: Solid State*, 1976, **13**, 5518–5529.
23 D. Graf, F. Molitor, K. Ensslin, C. Stampfer, A. Jungen, C. Hierold and L. Wirtz, *Nano Lett.*, 2007, **7**, 238–242.
24 W. Pan, J. Xiao, J. Zhu, C. Yu, G. Zhang, Z. Ni, K. Watanabe, T. Taniguchi, Y. Shi and X. Wang, *Sci. Rep.*, 2012, **2**, 893.
25 L. G. Cancado, A. Jori, E. H. M. Ferriera, F. Stavale, C. A. Achete, R. B. Capaz, M. V. O. Mountinho, A. Lombardo, T. S. Kulmala and A. C. Ferrari, *Nano Lett.*, 2011, **11**, 3190–3196.
26 S. O. Kasap, *Principles of Electronic Materials and Devices*, McGraw-Hill, New York, 3rd edn, 2006.
27 S. N. Cha, J. S. Seo, S. M. Kim, H. J. Kim, Y. J. Park, S. W. Kim and J. M. Kim, *Adv. Mater.*, 2010, **22**, 4726–4730.